https://doi.org/10.46813/2026-165-037

PRODUCT YIELDS OF THE PHOTOFISSION OF ^{232}Th BY 14.8 MeV BREMSSTRAHLUNG PHOTONS

V.V. Pyskach, O.O. Parlag, E.V. Oleinikov, A.N. Gomonai, I.V. Pylypchynets, A.I. Lengyel
Institute of Electron Physics, National Academy of Sciences of Ukraine, Uzhhorod, Ukraine
E-mail: v.pyskach@gmail.com

The relative (cumulative) yields of the products (^{85m}Kr, ^{87}Kr, ^{88}Kr, ^{91}Sr, ^{92}Sr, ^{97}Zr, ^{132}Te, ^{133}I, ^{135}I, ^{142}La, ^{143}Ce, ^{149}Nd) of ^{232}Th photofission induced by bremsstrahlung photons with a maximum energy of 14.8 MeV, generated using the M-30 microtron electron accelerator, are presented. The relative yields of ^{232}Th photofission products were determined by off-line gamma-ray spectrometry of an unseparated mixture of fragments collected in aluminium foils. The GEANT4 toolkit was used to simulate the irradiation conditions for inducing photofission. The experimental data exhibit a structure consistent with existing data at similar excitation energies and complement these data. The results confirm the presence of structure in the mass distributions of ^{232}Th photofission products associated with nuclear shell effects.

PACS: 24.75.+1, 25.85.-w, 25.85.Ec, 25.85.Ca

INTRODUCTION

Actinide fission product (fragment) yields are among the principal parameters characterising fission. Product mass-yield distributions provide information on the influence of nuclear structure and dynamics on the fission process [1]. Studies of nuclear photofission (photon-induced fission) product yields offer a promising approach to investigating fission, since the interaction of gamma rays with nuclei is purely electromagnetic. This simplifies the interpretation of the results and enables almost unambiguous conclusions to be drawn about the role of the effects under investigation [2, 3]. However, the experimental data currently available on actinide photofission product yields do not meet the requirements for developing theoretical models [4–9] or for practical applications [10].

This is particularly relevant to the ^{232}Th nucleus, which lies at the boundary between the pre-actinides ($_{89}$Ra) and the light actinides ($_{91}$Pa). Electromagnetic fission occurring in interactions involving relativistic radioactive beams and thorium isotopes (with mass numbers 221, 222, 225, 226, 229, and 230) exhibits a transition from symmetric to asymmetric fission. This is associated with differences in the probabilities of the symmetric and asymmetric fission channels and their influence on the formation of product mass distributions [11].

Experimental yield data for light and heavy ^{232}Th photofission products indicate fine structure in their mass distributions: enhanced yields of heavy products near mass numbers 133–134, 138–140, and 143–144, and of the corresponding complementary light products. This structure is associated with the effects of closed nuclear shells and odd–even staggering on fragment formation [12, 13]. Further studies of fine structure in fission product mass distributions are of interest for its experimental confirmation and theoretical description.

Photofission of ^{232}Th has a wide range of practical applications [14–21]. Product yield data are required for the development of next-generation energy systems [14, 15], accelerator-driven reactors (controlled subcritical systems) [16, 17], the transmutation of spent nuclear fuel [18], the production of neutron-rich radioactive beams [19, 20], and the development of non-destructive methods for the isotopic analysis of fertile nuclear materials [21]. In addition, fragment yield data are needed to develop Bayesian neural networks and models for predicting photofission product yields where data are absent or sparse [22].

These applications of ^{232}Th photofission require reliable yield information for a wide range of products and energies.

The experimental data currently available on ^{232}Th photofission product yields in the giant dipole resonance energy region differ, even when the numerical values were obtained at similar excitation energies using the same types of experimental methods [23, 24].

Experimental studies of ^{232}Th photofission product yields therefore remain an important research task.

This work reports the first experimental determination of the relative yields of 12 products of ^{232}Th photofission induced by bremsstrahlung with an endpoint energy of 14.8 MeV.

1. MATERIALS AND METHODS

The relative yields of ^{232}Th photofission products were determined by semiconductor gamma-ray spectrometry of an unseparated mixture of photofission fragments collected in aluminium foil [23, 25].

1.1. INDUCING ^{232}Th PHOTOFISSION AT THE M-30 MICROTRON

Seven ^{232}Th samples, each 12 mm in diameter and 2 μm thick, with masses ranging from 209 to 281 μg, were used in the experiments.

To collect photofission products during irradiation of the ^{232}Th samples, aluminium foils (collectors), 12 mm in diameter and 0.2 mm thick, were placed in direct contact with the ^{232}Th fission targets.

The fission assembly was irradiated at the M-30 microtron electron accelerator of the Institute of Electron Physics, NAS of Ukraine [26]. The electron energy was 14.8 MeV, the average beam current was approximately 4 μA, and electron energy fluctuations during irradiation did not exceed 0.04 MeV. Bremsstrahlung was generated using a tantalum converter placed 22 mm from the exit window of the electron extraction unit. The fission

assembly was positioned perpendicular to the beam axis, 50 mm from the converter. The irradiation time (Tir.) ranged from 0.5 to 2.0 h.

The irradiation arrangement for the fission assembly at the M-30 microtron is shown in Fig. 1, where 1 – electron extraction unit; 2 – titanium exit window (elliptical, with axis lengths of 22 and 6 mm and a thickness of 50 μm); 3 – tantalum converter (a rectangular plate measuring 100×50 mm and 1 mm thick); 4 – fission assembly comprising seven ^{232}Th foils (5) and aluminium collector foils (6).

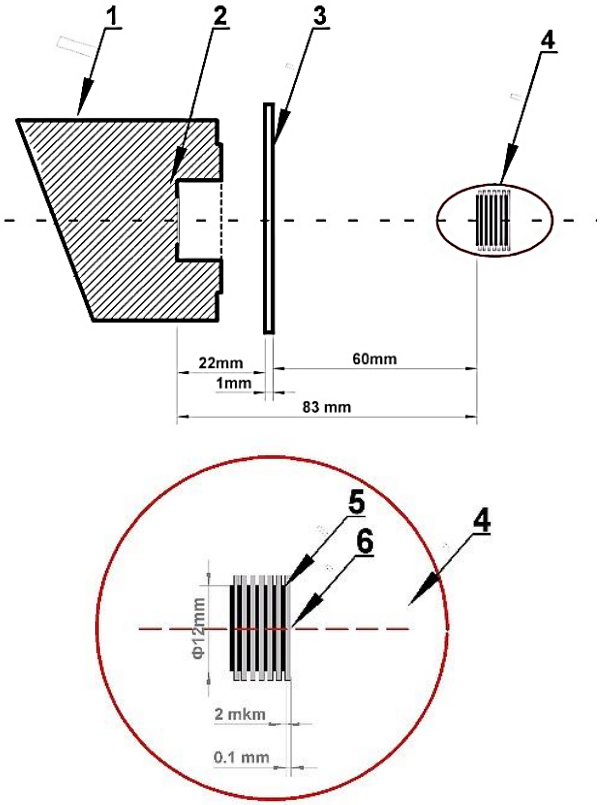


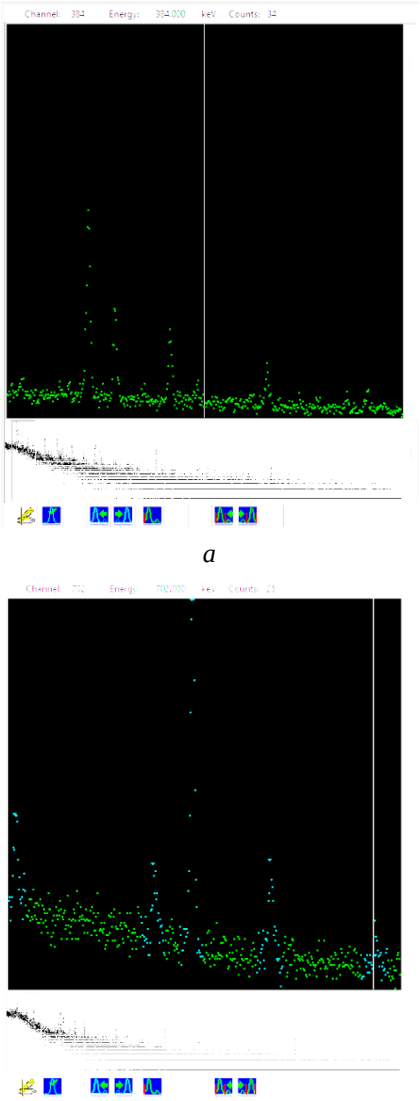
Fig. 1. Irradiation arrangement for the fission assembly at the M-30 microtron

1.2. GAMMA-RAY SPECTROMETRY OF ^{232}Th PHOTOFISSION PRODUCTS

Following irradiation of the fission assembly, spectrometric measurements were made of the delayed gamma radiation emitted by ^{232}Th photofission products collected in the aluminium foils. HPGe and Ge(Li) detectors with volumes of 150 and 100 cm^3, respectively, were used [23]. Standard certified point gamma-ray sources (^{22}Na, ^{57}Co, ^{60}Co, ^{109}Cd, ^{133}Ba, ^{137}Cs, ^{151}Eu, ^{241}Am) were used to determine the full-energy peak efficiencies of the detectors. The detectors were also self-calibrated using gamma radiation from photofission products collected in aluminium foil [23, 27]. This simplified the measurements and the processing of spectrometric data by accounting for the actual measurement geometry. The statistical uncertainty of the calibration measurements did not exceed 4%.

Measurements were performed at cooling times (Tc) ranging from 0.25 to 120 h after the end of irradiation, in live-time mode; the spectrometer dead time did not exceed 2%. The duration of individual measurements (Tm) ranged from 0.5 to 2 h.

Fig. 2 shows portions of the gamma-ray spectra of ^{232}Th photofission products (screenshots from the Winspectrum analysis software).



a

b

Fig. 2. Portions of the gamma-ray spectra of ^{232}Th photofission products (a – Tir = 2 h, Tc = 4 h, Tm = 1 h; b – Tir = 2 h, Tc = 18 h, Tm = 2 h)

The measured gamma-ray spectra were analysed using the Winspectrum software package [28].

The ^{232}Th photofission products were identified from their characteristic gamma-ray energies, taking into account their half-lives and those of their precursors in the isobaric decay chains [29, 30]. The irradiation, cooling and measurement times were also taken into account.

The time dependence of the intensities of the following gamma-ray lines of ^{232}Th photofission products was measured: ^{85m}Kr (151.2 [75.2]), ^{87}Kr (402.6 [50.0]), ^{88}Kr (196.3 [26.0]), ^{91}Sr (1024.3 [33.0]), ^{92}Sr (1383.9 [90.0]), ^{97}Zr (743.4 [50.0]), ^{132}Te (228.2 [88.0]), ^{133}I (529.9 [87.0]), ^{135}I (1260.4 (28.7)), ^{142}La (641.3 (47.4)), ^{143}Ce (293.3 (42.8)), ^{149}Nd (211.3 (25.9)). The energies of the gamma-ray lines used for analysis (keV) are given in parentheses and their intensities (%) in square brackets.

The statistical uncertainty in the measured intensities of gamma-ray lines from ^{232}Th photofission products did not exceed 3…5% throughout the measurement period.

1.3. SIMULATION OF FISSION ASSEMBLY ACTIVATION AT THE M-30 MICROTRON

The GEANT4 10.7 nuclear Monte Carlo code [31] was used to calculate the parameters (energy spectra and their integrals) of the components of the bremsstrahlung beam generated by the tantalum converter at the M-30 microtron: bremsstrahlung photons, residual electrons and secondary photoneutrons incident on the ^{232}Th samples. The input parameters fully reproduced the design of the electron extraction unit and the fission assembly activation arrangement used at the M-30 microtron electron accelerator [32, 33].

The simulated energy spectra of bremsstrahlung photons incident on the ^{232}Th samples for the irradiation arrangement used are shown in Fig. 3. The same figure also presents the cross-sections for the ^{232}Th(γ,f), ^{232}Th(γ,n)^{231}Th, and ^{231}Th(γ,f) reactions, using numerical values from the TENDL-2023 library [34].

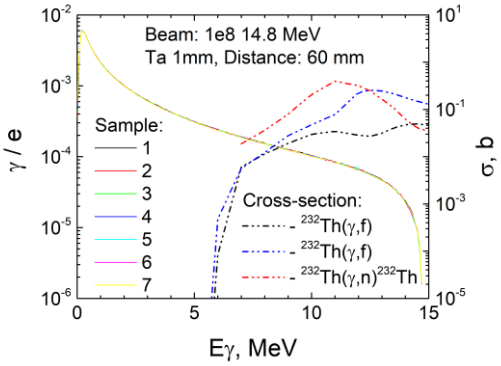


Fig. 3. Bremsstrahlung photon energy spectra and the ^{232}Th(γ,f) reaction cross-section [34]

The integrated photon flux incident on the fission assembly, calculated using equation (1) in [33] and normalised per primary electron, is 7.99E-2 photons (9.21E-3 for photon energies > 6 MeV).

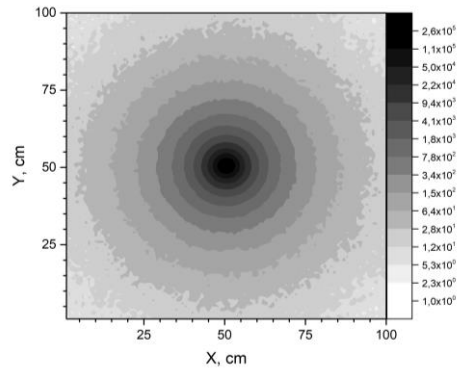


Fig. 4. Photon profile in the assembly plane

The simulations yielded the bremsstrahlung photon profile in a 100×100 mm plane at the position of the fission assembly (Fig. 4), together with the transverse photon distribution (Fig. 5).

The total number of photons incident on this plane is 1.90083E6; 537948 photons reach the target, corresponding to 28.3% of the total.

Figs. 6 and 7 show the energy spectra of residual electrons and secondary photoneutrons incident on the ^{232}Th assembly. Fig. 7 also shows the ^{232}Th(n,f) cross-section from the ENDF/B-VIII.1 library [34].

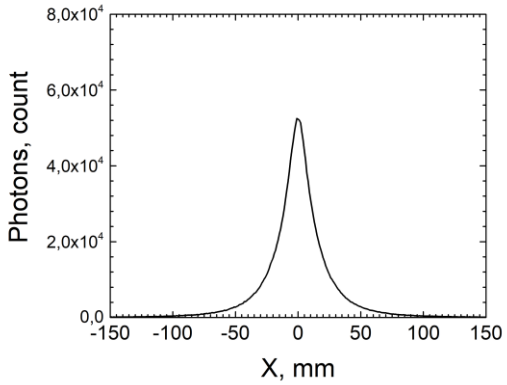


Fig. 5. Transverse photon distribution at the assembly

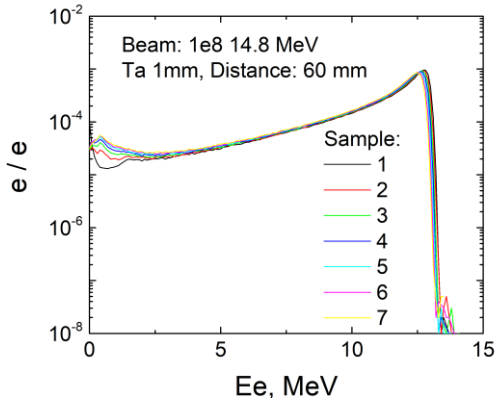


Fig. 6. Energy spectrum of residual electrons

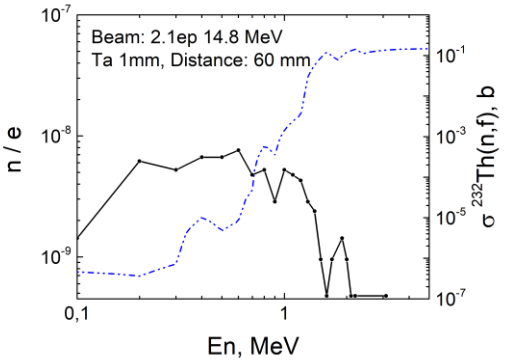


Fig. 7. Neutron energy spectrum and the ^{232}Th(n,f) reaction cross-section [34]

The integrated fluxes of residual electrons and secondary photoneutrons incident on the ^{232}Th sample, normalised per primary electron, are 1.73E-2 electrons (1.53E-2 for electron energies > 6 MeV) and 7.38E-8 photoneutrons, respectively.

These results were used to estimate the contributions of products from competing nuclear reactions (^{232}Th(γ,n)^{231}Th → ^{231}Th(γ,f) and ^{232}Th(n,f)) to the ^{232}Th photofission product yields during the 2 h irradiation of the fission assembly. All calculated values were normalised per primary electron (Fig. 8). The number of ^{231}Th nuclei produced via the (γ,n) reaction channel is 7.46598E-25. The numbers of photofission events in ^{232}Th and ^{231}Th and neutron-induced fission events in

^{232}Th during the 2 h irradiation are 1.14011E-25, 2.59386E-49 and 1.12391E-30, respectively.

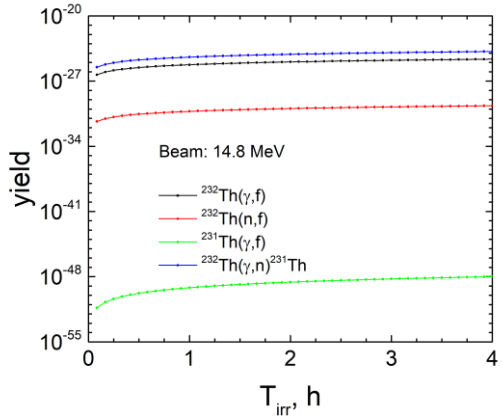


Fig. 8. Nuclear reaction product yields during irradiation of the fission assembly

The analysis indicates that product yields from competing reactions do not affect the accuracy of the final results.

The mean excitation energy of the fissioning ^{232}Th nucleus, calculated according to [35] for the photofission process, is 9.72 MeV.

2. RESULTS

The experiments yielded the following relative (cumulative) yields for 12 products of ^{232}Th photofission: ^{85m}Kr – 1.17, ^{87}Kr – 1.11, ^{88}Kr – 1.31, ^{91}Sr – 1.26, ^{92}Sr – 1.13, ^{97}Zr – 0.87, ^{132}Te – 0.78, ^{133}I – 1.0, ^{135}I – 1.20, ^{142}La – 1.32, ^{143}Ce – 1.48, ^{149}Nd – 0.34. The product yields were determined relative to the yield of ^{133}I.

The uncertainties in the relative photofission product yields were determined by taking into account the statistical uncertainties in the gamma-ray peak intensities, the analysis of their time dependence, and the uncertainties in the interpolated detector efficiencies and nuclear data. The total uncertainty in the relative yields of ^{232}Th photofission products did not exceed 12%.

The relative yields of ^{232}Th photofission products are shown by black circles in Fig. 9. Red circles show the normalised product yields, obtained by normalising the relative yields to Y(A=133) = 4.53%. This enables comparison with existing experimental data at similar excitation energies, denoted by diamonds [36], squares [37], stars [38], upward-pointing triangles [39] and downward-pointing triangles [40], and with a Bayesian neural network description of the yields (solid line) [22]. The structure of our data agrees with the existing data within experimental uncertainties over almost the entire mass range of ^{232}Th photofission products.

The blue dashed line in Fig. 9 shows the product mass-yield distribution simulated using the GEF 2025/1.3 nuclear Monte Carlo code [41] for the fissioning ^{232}Th* nucleus at an excitation energy of approximately 10 MeV. The GEF model does not reproduce the observed features of the photofission product yields at this excitation energy of the fissioning ^{232}Th nucleus.

A multi-Gaussian model (a superposition of three Gaussians) [35] was used to analyse the structure of the mass distribution of heavy ^{232}Th photofission products. The distribution was described using equation (1) from [35]:

$$Y_i(A) = \sum_{i=1}^{3} \frac{W_i}{\sqrt{2\pi}\sigma_{A,i}} exp\left(-\frac{(A-A_{H,i})^2}{2\sigma_{Ai}^2}\right), \qquad (1)$$

where $A_{H,i}$ are the most probable heavy-fragment masses; σ_{Ai} are the dispersions of the fragment mass distributions; and W_i are the probabilities of the individual fission channels (or the areas under the Gaussians), with centres near the most probable heavy-fragment masses (~ 133–134, ~ 138–139 and ~ 143–-144 [23, 36, 42]). In addition to our data, the analysis used existing experimental data obtained at similar excitation energies (see Fig. 9) [36–40].

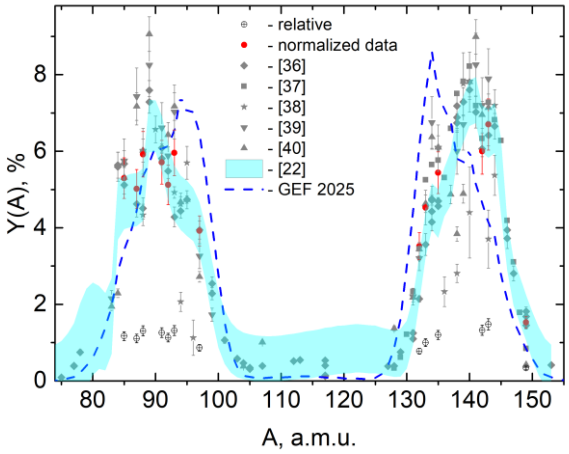


Fig. 9. Product yields from ^{232}Th photofission

Our calculations (Fig. 10) confirm the presence of three fine-structure peaks in the mass distribution of ^{232}Th photofission products, located near mass numbers 133–134, 138–139 and 143–144 and associated with nuclear shell effects.

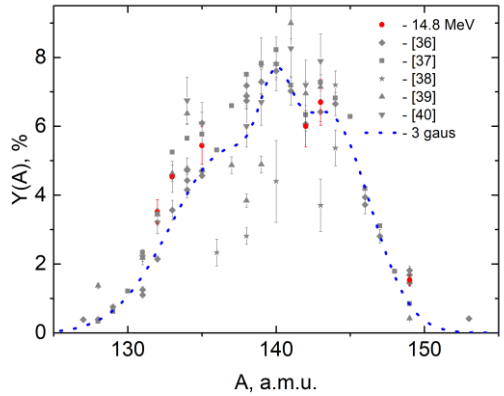


Fig. 10. Description of the experimental yields of heavy ^{232}Th photofission products by a superposition of three Gaussians

CONCLUSIONS

The relative (cumulative) yields of 12 products of ^{232}Th photofission – ^{85m}Kr, ^{87}Kr, ^{88}Kr, ^{91}Sr, ^{92}Sr, ^{97}Zr, ^{132}Te, ^{133}I, ^{135}I, ^{142}La, ^{143}Ce, and ^{149}Nd – have been determined for the first time at a bremsstrahlung endpoint energy of 14.8 MeV.

The yield data exhibit a structure consistent, within experimental uncertainties, with existing experimental data obtained at similar excitation energies and complement these data.

The analysis of our data and existing experimental heavy-product yields at an excitation energy of approximately 10 MeV, within a multimodal model describing the heavy-fragment distribution as a superposition of three Gaussians, confirms the presence of structure in the mass distributions of heavy ^{232}Th photofission products.

The experimental data can also be used to develop a Bayesian neural network (machine learning) model to describe fragment yields in the photofission of thorium isotopes.

ACKNOWLEDGEMENTS

The authors express their gratitude to the microtron group (Y. Gainish, G. Pitchenko, O. Turkhovsky) for the uninterrupted operation of the accelerator and to I. Kushtan for the technical support of the experimental studies.

This work was carried out within the framework of the topic "Implementation of simulation technologies into experimental studies of photofission of the ^{232}Th nucleus" State Registration No: 0126U002601.

REFERENCES

1. L. Csige, D.M. Filipescu. *Photofission studies: Past and future* / I. Tanihata, H. Toki, T. Kajino (eds): Handbook of Nuclear Physics. Springer, Singapore. 2022, p. 867-900; https://doi.org/10.1007/978-981-15-8818-1_81-1

2. T. Mukhopadhyay, D.N. Basu. Photonuclear reactions of actinides in the giant dipole resonance region // *The European Physical Journal A.* 2010, v. 45, p. 121-124; https://doi.org/10.1140/epja/i2010-10993-y

3. T. Mukhopadhyay, D.N. Basu. Photonuclear reactions of actinide and pre-actinide nuclei at intermediate energies // *Physical Review C.* 2007, v. 76, p. 064610; https://doi.org/10.1103/PhysRevC.76.064610

4. M. Bender, R. Bernard, G. Bertsch, et al. Future of nuclear fission theory // *Journal of Physics G*. 2020, v. 47, p. 113002; https://doi.org/10.1088/1361-6471/abab4f

5. I.A. Pshenichnov, B.L. Berman, W.J. Briscoe, et al. Intranuclear-Cascade model calculation of photofission probabilities for actinide nuclei // *The European Physical Journal A.* 2005, v. 24, p. 69-84; https://doi.org/10.1140/epja/i2004-10130-9

6. P.M. Kaldiani. The perusal of photofission fragments mass yields for actinide isotopes by systematics neutron models // *Phys. Atom. Nuclei.* 2019, v. 82, p. 450-461; https://doi.org/10.1134/S1063778819050089

7. V.T. Maslyuk, O.O. Parlag, M.I. Romanyuk, et al. Transformations of actinides fission product yields due to post-scission emission of nuclear particles: ^{232}Th // *Canadian Journal of Physics.* 2021, v. 99, p. 1007-1013; https://doi.org/10.1139/cjp-2020-0356

8. G.-L. Wang, H.-Y. Lan, X.-M. Shi, et al. A general framework for describing photofission observables of actinides at an average excitation energy below 30 MeV // *Chinese Physics C.* 2022, v. 46, p. 084102; https://doi.org/10.1088/1674-1137/ac6abc

9. Xiao-Ming Shi, Guan-Lin Wang, Kai-Jun Luo, et al. Geant4 development for actinides photofission simulation // *Nuclear Instruments and Methods in Physics Research A.* 2024, v. 1062, p. 169222; https://doi.org/10.1016/j.nima.2024.169222

10. K. Kolos, V. Sobes, R. Vogt, et al. Current nuclear data needs for applications // *Physical Review Research.* 2022, v. 4, p. 021001; https://doi.org/10.1103/PhysRevResearch.4.021001

11. A. Chatillon, J. Taïeb, H. Alvarez-Pol, et al. Experimental study of nuclear fission along the thorium isotopic chain: From asymmetric to symmetric fission // *Phys Rev C.* 2019, v. 99, p. 054628; https://doi.org/10.1103/PhysRevC.99.054628

12. H. Naik, S. Ganesan, M. Lee, et al. Yields of fission products in the gamma induced fission of preactinides and actinides // *Journal of the Korean Physical Society.* 2011, v. 59(2), p. 1848-1851; https://doi.org/10.3938/jkps.59.1848

13. P. Morfouace, J. Taïeb, A. Chatillon, et al. An asymmetric fission island driven by shell effects in light fragments // *Nature*. 2025, v. 641, p. 339-344; https://doi.org/10.1038/s41586-025-08882-7

14. R.K. Jyothi, L.G.T. Costa De Melo, R.M. Santos, H.-S. Yoon. An overview of thorium as a prospective natural resource for future energy // *Frontiers in Energy Research, Sec. Nuclear Energy*. 2023, v. 11, p. 1132611; https://doi.org/10.3389/fenrg.2023.1132611

15. N. Alnassar, A. A. Galahom. Investigating the potential advantages of using thorium-based fuel as an advanced nuclear fuel in a typical boiling water reactor assembly (BWR) // *Scientific Reports*. 2025, v. 15, p. 39772; https://doi.org/10.1038/s41598-025-23492-z

16. L. Sajo-Bohus, E.D. Greaves, J. Davila, et al. Th and U fuel photofission study by NTD for AD-MSR subcritical assembly // *AIP Conference Proceedings.* 2015, v. 1671, p. 020009; https://doi.org/10.1063/1.4927186

17. R. Yoshioka, K. Furukawa, M. Kinoshita, et al. *Chapter 15 – Accelerator-driven systems* / Editor(s): T.J. Dolan, I. Pázsit, A. Rykhlevskii, R. Yoshioka, In Woodhead Publishing Series in Energy, Molten Salt Reactors and Thorium Energy (Second Edition), Woodhead Publishing, 2024, p. 741; https://doi.org/10.1016/B978-0-323-99355-5.00001-X

18. M. Hu, M.W. Krasny, W. Płaczek, et al. Efficient transmutation of long-lived fission products in a Gamma Factory beam driven advanced nuclear energy system // *Scientific Reports*. 2025, v. 15, p. 12562; https://doi.org/10.1038/s41598-025-96505-6

19. S. Essabaa, N. Barré-Boscher, M.C. Mhamed, et al. The radioactive beam facility ALTO // *Nuclear Instruments and Methods in Physics Research Section B.* 2013, v. 317, p. 218-222; https://doi.org/10.1016/j.nimb.2013.06.029

20. P. Constantin, D.L. Balabanski, P.V. Cuong. Simulation of photofission experiments at the ELI-NP facility // *Nuclear Instruments and Methods in Physics Research Section B*. 2016, v. 372, p. 78-85; https://doi.org/10.1016/j.nimb.2016.02.004

21. I.V. Pylypchynets, O.O. Parlag, V.T. Maslyuk, et al. Isotopic identification of photofissed nuclear materials in stainless steel containers using delayed gamma-rays // *Problems of Atomic Science and Techno-*

logy. Series "Nuclear Physics Investigations". 2022, N 5(141), p. 103-109; https://doi.org/10.46813/2022-141-103

22. M.D. Zhou, C.Y. Qiao, P. Jiao, et al. Bayesian evaluation of photofission product yields of Th isotopic chains // *Nuclear Science and Techniques*. 2026, v. 37, p. 130; https://doi.org/10.1007/s41365-026-01951-0

23. O.O. Parlag, V.T. Maslyuk, E.V. Oleynikov, et al. Structure of mass-yield distributions of ^{232}Th photofission product by bremsstrahlung at energy 17.5 MeV // *Scientific Herald of Uzhhorod University. Series Physics*. 2021, v. 49, p. 54-60; https://doi.org/10.54919/2415-8038.2021.49.54-60

24. Experimental Nuclear Reaction Data (EXFOR). Database Version of 2026-08-27. Available from: https://www-nds.iaea.org/exfor/

25. Yu.V. Kibkalo, K.K. Kisurin, V.S. Semenov, et al. Fission fragments mass distributions in 238U+p interaction at energies up to 70 MeV // *Nuclear Physics and Atomic Energy.* 2006, v. 7(1), p. 30-34; https://doi.org/10.15407/jnpae2006.01.030

26. S. Kim, C.J. Martoff, M. Dion, D. Glasgow. Cumulative fission yields of short-lived fission products from ^{235}U and ^{239}Pu measured by HPGe gamma-ray spectroscopy // *Nuclear Instruments and Methods in Physics Research A*. 2024, v. 1059, p. 169001; https://doi.org/10.1016/j.nima.2023.169001

27. O.O. Parlag, V.T. Maslyuk, A.M. Dovbnya, et al. *Method for producing a multinuclide gamma-ray source for absolute efficiency calibration of semiconductor detectors:* Ukrainian utility model patent No. 130235 (Bulletin No. 22, 26 November 2018); https://iprop-ua.com/inv/i37tf6l8/

28. M.V. Strilchuk. User manual for Winspectrum. KINR NAS of Ukraine (unpublished). Private communication.

29. J. Blachot, C. Fiche. Gamma-ray and half-life data for the fission products // *Atomic Data and Nuclear Data Tables.* 1977, v. 20, p. 241-310; https://doi.org/10.1016/0092-640X(77)90002-X

30. Decay Radiation database version of 12/12/2025. Available from: https://www.nndc.bnl.gov/nudat3/indx_dec.jsp

31. GEANT4 11.1 (9 December 2022). Available from: https://geant4. web.cern.ch/support/download

32. O.O. Parlag, V.V. Pyskach, E.V. Oleinikov, et al. Modeling the characteristics of photons and residual electrons in bremsstrahlung beams generated by a tantalum converter on the M-30 microtron // *Problems of Atomic Science and Technology. Series "Nuclear Physics Investigations".* 2025, N 3(157), p. 169-175; https://doi.org/10.46813/2025-157-169

33. E.V. Oleinikov, I.V. Pylypchynets, O.O. Parlag, V.V. Pyskach. Photon and photoneutron outputs simulation from a tantalum converter at the M-30 microtron // *Problems of Atomic Science and Technology. Series "Nuclear Physics Investigations".* 2024, N 5(153), p. 148-153; https://doi.org/10.46813/2024-153-148

34. Evaluated Nuclear Data File (ENDF). Database Version of 2026-01-09. Available from: https://www-nds.iaea.org/exfor/endf.htm

35. E.V. Oleynikov, O.O. Parlag, I.V. Pylypchynets, et al. Structure of mass distributions of photofission product yields of ^{238}U at 17.5 MeV bremsstrahlung energy // *Problems of Atomic Science and Technology. Series "Nuclear Physics Investigations".* 2023, N 3(145), p. 26; https://doi.org/10.46813/2023-145-026

36. H. Naik, G.N. Kim, R. Schwengner, et al. Fission product yield distribution in the 12, 14, and 16 MeV bremsstrahlung-induced fission of ^{232}Th // *The European Physical Journal A*. 2015, v. 51, p. 150; https://doi.org/10.1140/epja/i2015-15150-8

37. K. Persyn, E. Jacobs, S. Pommé, et al. Excitation energy dependence of fragment characteristics for the photofission of ^{232}Th // *Nuclear Physics A.* 1997, v. 620, p. 171-190; https://doi.org/10.1016/S0375-9474(97)00156-5

38. A. Foley, H. Yang. Short-lived photofission product yields from ^{238}U and ^{232}Th at Bremsstrahlung X-ray endpoint energies of 8, 14, and 20 MeV for nuclear forensics isotope production applications // *Nuclear Inst. and Methods in Physics Research A.* 2021, v. 1013, p. 165621.

39. J.C. Hogan, A.E. Richardson, J.L. Meason, H.L. Wright. Photofission of ^{232}Th with 9, 15, and 38 MeV peak bremsstrahlung // *Physical Review C.* 1977, v. 16, p. 2296; https://doi.org/10.1103/PhysRevC.16.2296

40. N.N. Son, T.D. Thiep, P.V. Cuong. Structure effects in photofission // *Communications in Physics.* 2003, v. 113, p. 211; https://vjs.ac.vn/cip/article/view/2029/pdf%28Vietnamese%29

41. GEF 2025/1.3. (A General Description of Fission Observables). Available from: https://www.khschmidts-nuclear-web.eu/GEF-2025-1-3.htm

42. C. Agarwal, A. Goswami, P.C. Kalsi, et al. Mass yields in ^{229}Th(n,f) // *Journal of Radioanalytical and Nuclear Chemistry.* 2008, v. 275, p. 445-451; https://doi.org/10.1007/s10967-007-7011-8

Article received 21.09.2026

ВИХОДИ ПРОДУКТІВ ФОТОПОДІЛУ ^{232}Th ГАЛЬМІВНИМИ ФОТОНАМИ З ЕНЕРГІЄЮ 14,8 МеВ

В.В. Пискач, О.О. Парлаг, Є.В. Олейніков, Г.М. Гомонай, І.В. Пилипчинець, О.І. Лендел

Представлено значення відносних (кумулятивних) виходів продуктів (^{85m}Kr, ^{87}Kr, ^{88}Kr, ^{91}Sr, ^{92}Sr, ^{97}Zr, ^{132}Te, ^{133}I, ^{135}I, ^{142}La, ^{143}Ce, ^{149}Nd) фотоподілу ^{232}Th при енергії гальмівних фотонів 14,8 МеВ (які були згенеровані на електронному прискорювачі – мікротроні М-30). Визначення відносних виходів продуктів фотоподілу ^{232}Th здійснювалось методом off-line гамма-спектрометрії несепарованої суміші уламків, накопичених у алюмінієвих фольгах. Для моделювання процесу стимуляції реакції фотоподілу був використаний інструментарій GEANT4. Отримані експериментальні дані структурно узгоджуються з існуючими при близьких енергіях збудження і доповнюють їх. Експериментальні дані підтверджують наявність структури масових розподілів продуктів фотоподілу ^{232}Th, пов'язаної з впливом ядерних оболонок.